

# An $O(N)$ algorithm for constructing the solution operator to 2D elliptic boundary value problems in the absence of body loads

A. Gillman<sup>1</sup>, and P.G. Martinsson<sup>2</sup>

<sup>1</sup> Department of Mathematics, Dartmouth College, <sup>2</sup> Department of Applied Mathematics, University of Colorado at Boulder

**Abstract:** The large sparse linear systems arising from the finite element or finite difference discretization of elliptic PDEs can be solved directly via, e.g., nested dissection or multifrontal methods. Such techniques reorder the nodes in the grid to reduce the asymptotic complexity of Gaussian elimination from  $O(N^2)$  to  $O(N^{1.5})$  for typical problems in two dimensions. It has recently been demonstrated that the complexity can be further reduced to  $O(N)$  by exploiting structure in the dense matrices that arise in such computations (using, e.g.,  $\mathcal{H}$ -matrix arithmetic). This paper demonstrates that such *accelerated* nested dissection techniques become particularly effective for boundary value problems without body loads when the solution is sought for several different sets of boundary data, and the solution is required only near the boundary (as happens, e.g., in the computational modeling of scattering problems, or in engineering design of linearly elastic solids). In this case, a modified version of the accelerated nested dissection scheme can execute any solve beyond the first in  $O(N_{\text{boundary}})$  operations, where  $N_{\text{boundary}}$  denotes the number of points on the boundary. Typically,  $N_{\text{boundary}} \sim N^{0.5}$ . Numerical examples demonstrate the effectiveness of the procedure for a broad range of elliptic PDEs that includes both the Laplace and Helmholtz equations.

## 1. INTRODUCTION

**1.1. Problem formulation.** This paper presents a fast solver for homogeneous boundary value problems (BVPs) of the form

$$(1) \quad \begin{aligned} -\Delta u(\mathbf{x}) + b(\mathbf{x})u_x(\mathbf{x}) + c(\mathbf{x})u_y(\mathbf{x}) + d(\mathbf{x})u(\mathbf{x}) &= 0 & \mathbf{x} \in \Omega \\ u(\mathbf{x}) &= g(\mathbf{x}) & \mathbf{x} \in \Gamma, \end{aligned}$$

where  $\Omega = [0, 1]^2$  is the unit square in  $\mathbb{R}^2$ , where  $\Gamma$  is the boundary of  $\Omega$ , and where  $b$ ,  $c$ , and  $d$  are functions on  $\Omega$ . We assume that the only information sought is the normal derivative of  $u$  at  $\Gamma$ . In other words, the objective is to construct an approximation to the Dirichlet-to-Neumann operator associated with the elliptic differential operator in (1).

The proposed solver is particularly efficient for situations where (1) needs to be solved for a sequence of different boundary data functions  $g$ . The solver has two steps: (1) Build the approximate Dirichlet-to-Neumann operator for a given set of functions  $b$ ,  $c$ , and  $d$ . (2) Determine the Neumann data  $\partial u / \partial n$  for any given Dirichlet data

$g$  by applying the approximate Dirichlet-to-Neumann operator. The key claim of the paper is that the “build stage” can be executed in  $O(N)$  operations, and the “solve stage” can be executed in  $O(N^{0.5})$  operations. In contrast, classical nested dissection requires  $O(N^{1.5})$  and  $O(N)$  operations for the two steps, respectively.

**1.2. Motivation.** While the present paper addresses the specific BVP (1) on a simple square domain, the technique can be extended for building solution operators to elliptic boundary value problems of the form

$$(2) \quad \begin{cases} Au(\mathbf{x}) = f(\mathbf{x}) & \mathbf{x} \in \Omega \\ Bu(\mathbf{x}) = g(\mathbf{x}) & \mathbf{x} \in \Gamma, \end{cases}$$

where  $\Omega$  is a domain in  $\mathbb{R}^2$  or  $\mathbb{R}^3$  with boundary  $\Gamma$ , where  $A$  is an elliptic partial differential operator, and where  $B$  is a trace operator (representing boundary conditions like Dirichlet, Neumann, mixed, etc.). The goal of this paper is to illustrate that when the body load  $f$  is zero and the solution  $u$  and/or its derivatives are sought only near the boundary, the relevant solution operator can be constructed at moderate cost, and applied almost instantaneously. This opens up the possibility of high accuracy computational simulations to be carried out in real time for 3D problems such as elasticity involving composite materials, electrostatics in domains with variable conductivity, acoustic and electromagnetic scattering problems (at long and intermediate wave-lengths at least), and many others.

In some applications such as seismic testing and automatic multilevel substructuring (AMLS), there is a small number of localized body loads inside of the domain. This paper details how the solution operator can be found with an increased cost which is still less than classic techniques.

**1.3. Discretization.** The method described is applicable to a variety of geometries and discretization schemes (finite elements, finite differences, etc.). For simplicity of presentation, we restrict our attention to the model problem where a square domain  $\Omega$  is discretized via a finite difference scheme on a regular  $n \times n$  square mesh. The resulting linear system takes the form

$$(3) \quad \mathbf{A}\mathbf{u} = \mathbf{b}$$

where  $\mathbf{A}$  is an  $n^2 \times n^2$  sparse matrix. We let  $N = n^2$  denote the total number of grid points.

*Example:* When (1) represents the Laplace equation ( $b = c = d = 0$ ) and the standard five-point finite difference stencil is used in the discretization,  $\mathbf{A}$  consists of  $n \times n$  blocks, each of size  $n \times n$ ,

$$\mathbf{A} = \begin{bmatrix} \mathbf{B} & -\mathbf{I} & 0 & 0 & \cdots \\ -\mathbf{I} & \mathbf{B} & -\mathbf{I} & 0 & \cdots \\ 0 & -\mathbf{I} & \mathbf{B} & -\mathbf{I} & \cdots \\ 0 & 0 & -\mathbf{I} & \mathbf{B} & \cdots \\ \vdots & \vdots & \vdots & \vdots & \ddots \end{bmatrix}, \quad \text{where } \mathbf{B} = \begin{bmatrix} 4 & -1 & 0 & 0 & \cdots \\ -1 & 4 & -1 & 0 & \cdots \\ 0 & -1 & 4 & -1 & \cdots \\ 0 & 0 & -1 & 4 & \cdots \\ \vdots & \vdots & \vdots & \vdots & \ddots \end{bmatrix},$$

and where  $\mathbf{I}$  is the  $n \times n$  identity matrix.

1.4. **Existing fast solvers.** There already exist many efficient techniques for solving (3), including:

*Iterative methods:* These techniques construct a sequence of successively more accurate approximate solutions by applying the matrix  $A$  to a sequence of vectors. Since the  $N \times N$  matrix  $A$  has  $O(N)$  non-zero entries, the resulting solver has  $O(N)$  complexity whenever convergence is fast. It is difficult to predict the convergence rate of iterative methods and often a customized pre-conditioner is required to accelerate the schemes.

*Multigrid methods:* These techniques can be viewed as a special case of iterative methods. They can in certain circumstances reach very high performance by decomposing the matrix in a sequence of different scales; since the matrix is well-conditioned on each scale, very fast convergence often results.

*Direct methods:* Direct solvers (such as Gaussian elimination) which compute a solution in a single shot are considered more stable and robust than iterative methods. Proper ordering of the nodes often allows Gaussian elimination to be executed at  $O(N^{1.5})$  complexity ([6]), and the resulting “nested dissection” approach is quite competitive for moderate problem sizes (up to about  $N \sim 10^6$ ). More recently, it has been shown that by exploiting additional structure in the coefficient matrix, the nested dissection method can be accelerated to (close to) linear complexity, see, e.g., [3, 10, 12].

1.5. **Novelty of the present work and comparison to existing methodology.** The proposed solver is based on the classical nested dissection algorithm of [6]. The key distinction to classical nested dissection is that special structure in the dense so called “frontal matrices” are exploited to reduce the cost of the pre-computation from  $O(N^{1.5})$  to  $O(N)$ , and the cost of the solve from  $O(N)$  to  $O(N^{0.5})$ . To be precise, we approximate off-diagonal blocks of the dense frontal matrices by low-rank matrices; we do this using the structured matrix format described in [4, 8], which can be viewed as a variation of the well established “ $\mathcal{H}$ -matrix” and “ $\mathcal{H}^2$ -matrix” formats of Hackbusch and co-workers (see, e.g., [9, 1]).

The observation that the dense matrix computations involving the frontal matrices can be accelerated using structured matrix algebra has recently been made in, e.g., [3, 10, 11, 12]. Our work is slightly different in that it is based on the hierarchical construction of Schur complements, and directly leads to a discrete approximation of the Dirichlet-to-Neumann operator on the full domain. This greatly simplifies the construction of the boundary-to-boundary solution operator. It also leads to algorithms that can readily handle a problem involving a sparse body load (see Section 7.3).

While the present work considers only a regular square grid in 2D, the method can be extended to more general grids, and to 3D problems. A discussion of the expected performance in these cases can be found in Section 8. Our key claims regarding asymptotic complexity are summarized in Table 1.

An early version of the work reported appeared in the Ph.D. dissertation [7].

**Remark 1.1.** State-of-the-art iterative solvers such as, e.g., multigrid will sometimes outperform the new accelerated nested dissection technique for a stand-alone solve. However, the new solver is much faster for

subsequent solves; its asymptotic cost is only  $O(N^{0.5})$  and its practical efficiency is such that a problem on a grid with  $4000 \times 4000$  nodes can be solved in only 0.1 seconds on a standard office laptop. Moreover, since the solver is direct, it handles with ease many problems that are challenging for iterative methods (including multigrid), such as for instance vibration problems in situations where the domain is much larger than the wave-length.

	Build solution operators	Solve with no body load	Solve with general body load
2D	$N$ ( $N^{3/2}$ )	$N^{1/2}$ ( $N$ )	$N$ ( $N \log N$ )
3D	$N^{4/3}$ ( $N^2$ )	$N$ ( $N^{4/3}$ )	$N \log N$ ( $N^{4/3} \log N$ )

TABLE 1. Summary of asymptotic costs of the proposed direct solver in two and three dimensions. For comparison, the costs of classical nested dissection are given in parenthesis. For special (e.g. sparsely supported) body loads, better asymptotics than those listed in the table can be achieved, see Section 7.3. The asymptotics given for 3D problems are predictions for a simplistic generalization of the proposed scheme; it is likely that these numbers could be further improved.

1.6. **Outline of paper.** The paper describes an  $O(N)$  variation of the nested dissection method which computes the global Dirichlet-to-Neumann operator. Section 2 describes a hierarchical partitioning of the grid into a quad-tree of nested boxes. Section 3 describes a variation of the classical nested dissection technique that computes a hierarchy of solution operators for each box in the quad-tree. The solution operators have internal structure (see Section 4) which is exploited to improve the complexity of the method from  $O(N^{1.5})$  to  $O(N)$ , see Sections 5 and 6. Section 7 reports the results of numerical experiments that substantiate our claims on the asymptotic complexity and accuracy of the method.

## 2. TREE STRUCTURE

The direct solver described in this note is based on the classical nested dissection algorithm, and uses an analogous (but not identical) tree structure on the computational grid. This section formally defines the tree structure for our simple model geometry.

Let  $\Omega$  denote the square domain introduced in Section 1, and suppose that it is discretized using a uniform  $n \times n$  grid. Let  $N = n^2$  denote the number of points in the grid, and let  $N_{\text{leaf}}$  denote a tuning parameter chosen so that a matrix of size  $N_{\text{leaf}} \times N_{\text{leaf}}$  can be inverted quickly by brute force. The optimal choice of  $N_{\text{leaf}}$  depends on the computing environment, but we have found that  $N_{\text{leaf}} = 4096$  is often a good choice. Let  $L$  be the smallest integer such that when  $\Omega$  is partitioned into  $4^L$  equisized boxes, each box contains no more than  $N_{\text{leaf}}$  points. These  $4^L$  small boxes are called the *leaves* of the tree. Merge the leaves by sets of fours

into boxes with twice the side length, to form the  $4^{L-1}$  boxes that make up the next level in the tree. This process is repeated until  $\Omega$  is recovered. We call  $\Omega$  the *root* of the tree.

The set consisting of all boxes of the same size forms what we call a *level*. We label the levels using the integer  $\ell = 0, 1, 2, \dots, L$ , with  $\ell = 0$  denoting the root, and  $\ell = L$  denoting the leaves.

### 3. A VARIATION OF THE NESTED DISSECTION ALGORITHM

This section describes a direct solver that is particularly fast for what we call “pure” boundary value problems such as (1) in which there is no body load, and where the solution is sought only near the boundary. The idea is to construct a solution operator  $\mathbf{G}$  that maps the given boundary data to the sought potential values (or flows) on the boundary. Letting  $N_b$  denote the number of nodes on the boundary of the domain,  $\mathbf{G}$  is a dense  $N_b \times N_b$  matrix.

Technically, the solution operator  $\mathbf{G}$  is constructed via a divide-and-conquer approach (analogous to the one used in the classical nested dissection scheme): First a solution operator is constructed for each “leaf” in the quadtree described in Section 2, then solution operators for larger boxes are constructed via a hierarchical merging process in a single sweep through the tree, going from smaller to larger boxes.

For a grid with  $N$  nodes, the process described in this section requires  $O(N^{1.5})$  operations to construct the solution operator, and then each subsequent solve (which consists merely of applying the solution operator) requires  $O(N)$  operations. Techniques for accelerating these two costs to  $O(N)$  and  $O(N^{0.5})$ , respectively, are then described in Sections 4, 5 and 6.

**3.1. The solution operator and the Schur complement.** This subsection provides a precise definition of the concept of a “solution operator” associated with a subdomain  $P$  of the computational grid. For simplicity, we assume that  $P$  is a square or rectangular domain. We partition  $P$  into interior nodes and boundary nodes:

$$P = P_i \cup P_b,$$

where  $P_i$  is defined as the set of nodes that have all four neighbors inside  $P$ , see Figure 1. (Note that the set  $P$  consists of all nodes at which the potential is unknown, and  $P_b$  is the outermost ring of these nodes, *not* the nodes at which Dirichlet data is prescribed.)

Let  $\mathbf{u}_b$  and  $\mathbf{u}_i$  denote the potentials at the boundary nodes and the interior nodes, respectively. Reordering the equilibrium equation (restricted to  $P$ ), we find that  $\mathbf{u}_b$  and  $\mathbf{u}_i$  must satisfy

$$(4) \quad \begin{bmatrix} \mathbf{A}_{b,b} & \mathbf{A}_{b,i} \\ \mathbf{A}_{i,b} & \mathbf{A}_{i,i} \end{bmatrix} \begin{bmatrix} \mathbf{u}_b \\ \mathbf{u}_i \end{bmatrix} = \begin{bmatrix} \mathbf{f}_b \\ \mathbf{f}_i \end{bmatrix}.$$

Eliminating  $\mathbf{u}_i$  from (4), we find

$$\mathbf{S} \mathbf{u}_b = \mathbf{f}_b - \mathbf{A}_{b,i} \mathbf{A}_{i,i}^{-1} \mathbf{f}_i,$$

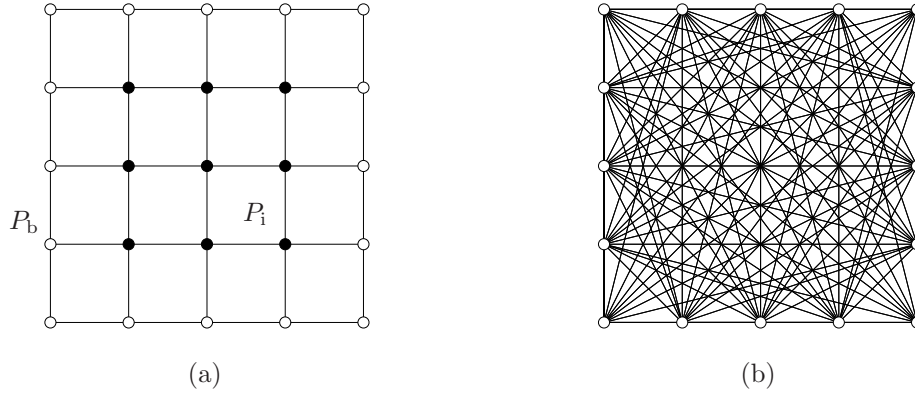


FIGURE 1. (a) Labeling of nodes for constructing the Schur complement of a leaf.  $P_i$  are the interior nodes (solid), and  $P_b$  are the boundary nodes (hollow). (b) After the merge, all internal nodes are “eliminated” but now all nodes communicate directly (i.e. the Schur complement  $S$  is dense).

where  $S$  is the matrix

$$(5) \quad S = A_{b,b} - A_{b,i} A_{i,i}^{-1} A_{i,b}.$$

We refer to  $S$  as the *Schur complement* associated with the subdomain  $P$ ; the *solution operator* is then  $G = S^{-1}$ . In the case of no body loads  $f_i = \mathbf{0}$ , thus the update to the right hand side on the boundary is not necessary.

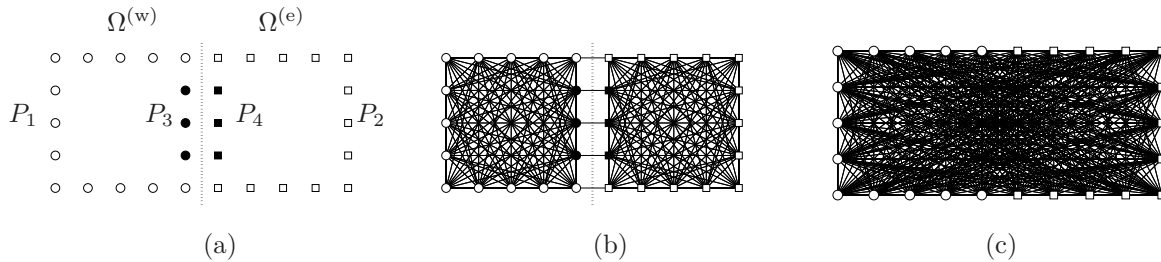


FIGURE 2. (a) Labeling of nodes for the merge operation described in Section 3. The nodes in  $P_1$  and  $P_3$  are round, and the nodes in  $P_2$  and  $P_4$  are square. The solid nodes are interior to the union of the two boxes  $\Omega^{(w)}$  and  $\Omega^{(e)}$ . (b) Connections between nodes before the merge. (c) Connections between nodes after eliminating the interior (solid) nodes.

**3.2. Merging two Schur complements.** In this section, we present a technique for merging the Schur complements for two adjacent boxes. Let us call the two boxes  $\Omega^{(w)}$  and  $\Omega^{(e)}$  (for “west” and “east”). Further, let  $P^{(w)}$  and  $P^{(e)}$  denote the nodes on the boundaries of these two boxes, and let  $S^{(w)}$  and  $S^{(e)}$  denote Schur complements supported on these two sets of boundary nodes, see Figure 2 (a).

The objective of the merge is to eliminate the nodes that are now “interior” to the larger box formed by the union of the two smaller boxes; these nodes are marked as blue in Figure 2 (b). To eliminate these points, we

first partition the nodes in  $P^{(w)}$  and  $P^{(e)}$  so that

$$(6) \quad P^{(w)} = P_1 \cup P_3, \quad \text{and} \quad P^{(e)} = P_2 \cup P_4,$$

and so that  $P_1 \cup P_2$  forms the boundary of the larger box, while the nodes in  $P_3 \cup P_4$  are interior, see Figure 2 (c). Partition the Schur complements  $S^{(w)}$  and  $S^{(e)}$  analogously:

$$S^{(w)} = \begin{bmatrix} S_{11} & S_{13} \\ S_{31} & S_{33} \end{bmatrix}, \quad \text{and} \quad S^{(e)} = \begin{bmatrix} S_{22} & S_{24} \\ S_{42} & S_{44} \end{bmatrix}.$$

Supposing that the right hand side has been updated to account for any interior body loads, equation (3) restricted to the union of the two boxes now reads

$$(7) \quad \left[ \begin{array}{cc|cc} S_{11} & A_{12} & S_{13} & A_{14} \\ A_{21} & S_{22} & A_{23} & S_{24} \\ \hline S_{31} & A_{32} & S_{33} & A_{34} \\ A_{41} & S_{42} & A_{43} & S_{44} \end{array} \right] \begin{bmatrix} \mathbf{u}_1 \\ \mathbf{u}_2 \\ \mathbf{u}_3 \\ \mathbf{u}_4 \end{bmatrix} = \begin{bmatrix} \mathbf{f}_1 \\ \mathbf{f}_2 \\ \mathbf{f}_3 \\ \mathbf{f}_4 \end{bmatrix},$$

where  $A_{ij}$  are the relevant sub-matrices of the original discrete Laplacian  $A$ . From (7), one finds that the Schur complement of the union box is

$$(8) \quad S = \begin{bmatrix} S_{11} & A_{12} \\ A_{21} & S_{22} \end{bmatrix} - \begin{bmatrix} S_{13} & A_{14} \\ A_{23} & S_{24} \end{bmatrix} \begin{bmatrix} S_{33} & A_{34} \\ A_{43} & S_{44} \end{bmatrix}^{-1} \begin{bmatrix} S_{31} & A_{32} \\ A_{41} & S_{42} \end{bmatrix}.$$

The updated right hand side is

$$\begin{bmatrix} \mathbf{f}_1 \\ \mathbf{f}_2 \end{bmatrix} - \begin{bmatrix} S_{13} & A_{14} \\ A_{23} & S_{24} \end{bmatrix} \begin{bmatrix} S_{33} & A_{34} \\ A_{43} & S_{44} \end{bmatrix}^{-1} \begin{bmatrix} \mathbf{f}_3 \\ \mathbf{f}_4 \end{bmatrix}.$$

**Remark 3.1.** The matrices  $A_{14}$ ,  $A_{23}$ ,  $A_{32}$ , and  $A_{41}$  are typically very sparse. In fact, when equation (1) is discretized with a 5-point stencil, these matrices are identically zero.

**Remark 3.2.** While the Schur complement is a dense matrix (cf. Figure 2), the interactions between distant points can to high precision be approximated by low rank matrices. This property can be conjectured by inspecting a computed Schur complement and observing that each row is smooth away from the diagonal. Figure (3) illustrates this point. The figure also illustrates that the Schur complement is strongly diagonal dominant, which is consistent with the fact that it is a discrete analog of the Dirichlet-to-Neumann operator, which is a hyper-singular integral operator (it *reduces* the smoothness of any boundary function it operates on in a manner similar to a differentiation operator).

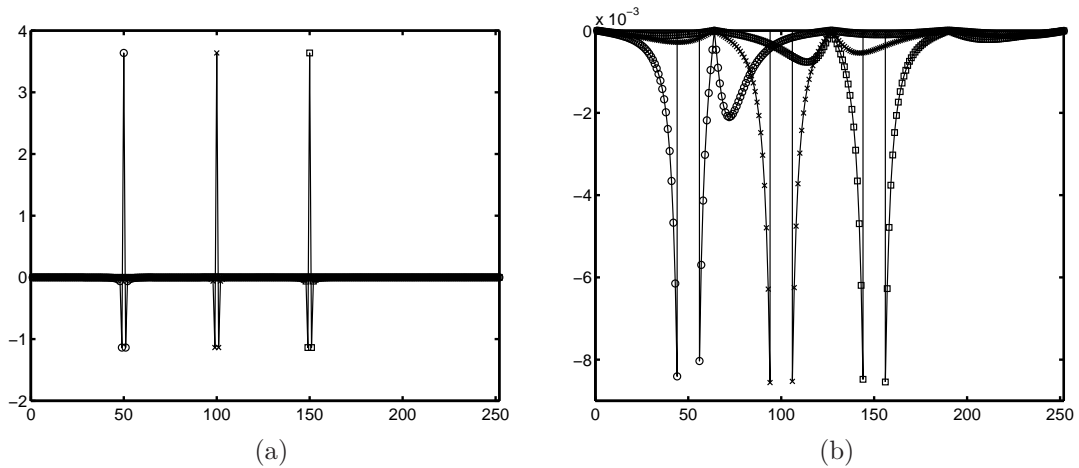


FIGURE 3. (a) Three rows of a typical Schur complement for a Laplace problem with 252 points on the boundary. The 50<sup>th</sup> (○), 100<sup>th</sup> (×), and 150<sup>th</sup> (□) rows are shown. Note how the matrix is completely dominated by the elements close to the diagonal. (b) The same plot but with a different scale on the vertical axis to show the smoothness in the far-field.

**3.3. The full algorithm.** For future reference, let us summarize the algorithm described:

- (1) *Construct a quad-tree:* Partition the grid into a hierarchy of boxes as described in Section 2.
- (2) *Process the leaves:* For each leaf box in the tree, construct its Schur complement as described in Section 3.1. If the box has body loads, update the right hand side.
- (3) *Hierarchical merge:* Loop over all levels of the tree, from finer to smaller. For each box on a level, compute its Schur complement by merging the (already computed) Schur complements of its children. Note that the merge of four children can be executed via three of the pair-wise merges described in Section 3.2. If the interior points have body loads, update the right hand side.
- (4) *Process the root of the tree:* After completing Step 3, the Schur complement for the entire domain is available. Invert (or factor) it to construct the solution operator.

**Remark 3.3.** For simplicity, the algorithm is described in a level-by-level manner (process all leaves first, then proceed one level at a time in going upwards). In fact, there is flexibility to travel through the tree in any order that ensures that no node is processed before its children. Since all Schur complements can be discarded once their information has been passed on to a parent, smarter orderings can greatly reduce the memory requirements [5].

**3.4. Asymptotic complexity of the algorithm.** As before, let  $N = n^2$  denote the total number of points in the grid, let  $N_{\text{leaf}}$  denote the maximum number of points on a leaf, and let  $L$  denote the number of levels so that  $N \leq 4^L N_{\text{leaf}}$ .



The cost to process one leaf in Step 2 in Section 3.3 is  $O(N_{\text{leaf}}^2)$  (exploiting that the matrix  $A_{i,i}$  in (5) is band-diagonal). Since there are  $4^L$  leaves, the total cost of Step 2 is therefore  $4^L N_{\text{leaf}}^2 \sim N N_{\text{leaf}}$ . Since  $N_{\text{leaf}}$  is a small constant number (in principle one could set  $N_{\text{leaf}} = 1$ ) the leaf processing cost is  $O(N)$ .

Next consider the cost of constructing the Schur complement of a box on level  $\ell$  in executing Step 3 in Section 3.3. Note that all boxes involved have  $O(n 2^{-\ell})$  points along each side. Since some matrices in (8) are dense, the cost for each merge is proportional to  $(n 2^{-\ell})^3 = n^3 2^{-3\ell}$ . Since we need to compute  $2^{2\ell}$  Schur complements on level  $\ell$ , the total cost of Step 3 is then  $\sum_{\ell=1}^L 2^{2\ell} n^3 2^{-3\ell} = n^3 \sum_{\ell=1}^L 2^{-\ell} \sim n^3$ .

Since the cost of the final inversion/factorization in Step 4 is  $O(n^3)$ , the total cost of the algorithm in Section 3.3 is  $O(n^3) = O(N^{1.5})$ .

#### 4. COMPRESSIBLE MATRICES

To improve the scaling of the nested dissection method, a more efficient technique for evaluating (8) will be implemented. We will exploit that while the matrices  $S_{ij}$  are all dense, they in the present context have additional structure:  $S_{ij}$  is when  $i \neq j$  to high precision rank deficient, and  $S_{ii}$  has a structure that we call *Hierarchically Block Separable (HBS)*. This section briefly describes the HBS property, for details see [8]. We note that the HBS property is very similar to the concept of *Hierarchically Semi-Separable (HSS)* matrices [13, 2] which has previously been used in an analogous context [3]. Other researchers have used the somewhat related  $\mathcal{H}$ -matrix concept for similar purposes [10, 12].

**4.1. Block separable.** Let  $H$  be an  $mp \times mp$  matrix that is blocked into  $p \times p$  blocks, each of size  $m \times m$ .

We say that  $H$  is “block separable” with “block-rank”  $k$  if for  $\tau = 1, 2, \dots, p$ , there exist  $m \times k$  matrices  $U_\tau$  and  $V_\tau$  such that each off-diagonal block  $H_{\sigma,\tau}$  of  $H$  admits the factorization

$$(9) \quad \begin{array}{ccccc} H_{\sigma,\tau} & = & U_\sigma & \tilde{H}_{\sigma,\tau} & V_\tau^* \\ m \times m & & m \times k & k \times k & k \times m \end{array}, \quad \sigma, \tau \in \{1, 2, \dots, p\}, \quad \sigma \neq \tau.$$

Observe that the columns of  $U_\sigma$  must form a basis for the columns of all off-diagonal blocks in row  $\sigma$ , and analogously, the columns of  $V_\tau$  must form a basis for the rows in all the off-diagonal blocks in column  $\tau$ . When (9) holds, the matrix  $H$  admits a block factorization

$$(10) \quad \begin{array}{ccccccc} H & = & U & \tilde{H} & V^* & + & D, \\ mp \times mp & & mp \times kp & kp \times kp & kp \times mp & & mp \times mp \end{array}$$

where

$$U = \text{diag}(U_1, U_2, \dots, U_p), \quad V = \text{diag}(V_1, V_2, \dots, V_p), \quad D = \text{diag}(D_1, D_2, \dots, D_p),$$

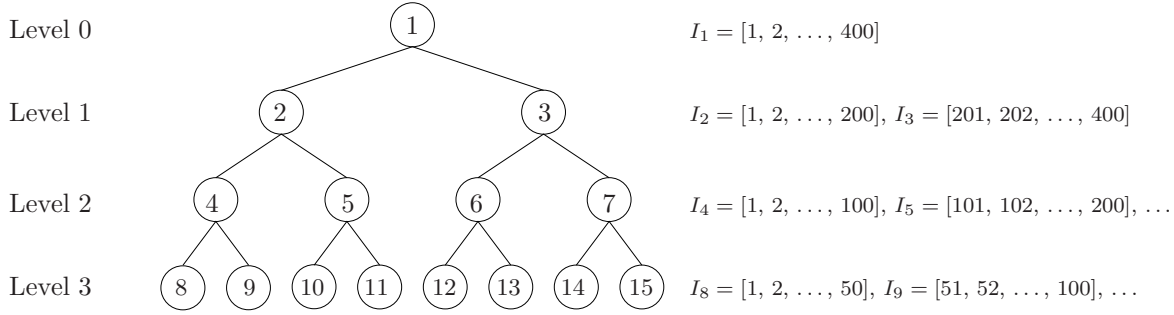


FIGURE 4. Numbering of nodes in a fully populated binary tree with  $L = 3$  levels. The root is the original index vector  $I = I_1 = [1, 2, \dots, 400]$ .

and

$$\tilde{\mathbf{H}} = \begin{bmatrix} 0 & \tilde{\mathbf{H}}_{12} & \tilde{\mathbf{H}}_{13} & \cdots \\ \tilde{\mathbf{H}}_{21} & 0 & \tilde{\mathbf{H}}_{23} & \cdots \\ \tilde{\mathbf{H}}_{31} & \tilde{\mathbf{H}}_{32} & 0 & \cdots \\ \vdots & \vdots & \vdots & \ddots \end{bmatrix}.$$

**4.2. Hierarchically Block-Separable.** Informally speaking, a matrix  $\mathbf{H}$  is *Hierarchically Block-Separable* (HBS), if it is amenable to a *telescoping* block factorization. In other words, in addition to the matrix  $\mathbf{H}$  being block separable, so is  $\tilde{\mathbf{H}}$  once it has been reblocked to form a matrix with  $p/2 \times p/2$  blocks. Likewise, the middle matrix from the block separable factorization of  $\tilde{\mathbf{H}}$  will be block separable, etc.

In this section, we describe properties and the factored representation of HBS matrices. Details on constructing the factorization are provided in [8].

**4.2.1. A binary tree structure.** The HBS representation of an  $M \times M$  matrix  $\mathbf{H}$  is based on a partition of the index vector  $I = [1, 2, \dots, M]$  into a binary tree structure. We let  $I$  form the root of the tree, and give it the index 1,  $I_1 = I$ . We next split the root into two roughly equi-sized vectors  $I_2$  and  $I_3$  so that  $I_1 = I_2 \cup I_3$ . The full tree is then formed by continuing to subdivide any interval that holds more than some preset fixed number  $m$  of indices. We use the integers  $\ell = 0, 1, \dots, L$  to label the different levels, with 0 denoting the coarsest level. A *leaf* is a node corresponding to a vector that never got split. For a non-leaf node  $\tau$ , its *children* are the two boxes  $\sigma_1$  and  $\sigma_2$  such that  $I_\tau = I_{\sigma_1} \cup I_{\sigma_2}$ , and  $\tau$  is then the *parent* of  $\sigma_1$  and  $\sigma_2$ . Two boxes with the same parent are called *siblings*. These definitions are illustrated in Figure 4.

**4.3. Definition of the HBS property.** We now define what it means for an  $M \times M$  matrix  $\mathbf{H}$  to be *hierarchically block separable* with respect to a given binary tree  $\mathcal{T}$  that partitions the index vector  $J = [1, 2, \dots, M]$ . For simplicity, we suppose that for every leaf node  $\tau$  the index vector  $I_\tau$  holds precisely  $m$  points, so that  $M = m2^L$ . Then  $\mathbf{H}$  is HBS with block rank  $k$  if the following two conditions hold:

	Name:	Size:	Function:
For each leaf node $\tau$ :	$D_\tau$	$m \times m$	The diagonal block $H(I_\tau, I_\tau)$ .
	$U_\tau$	$m \times k$	Basis for the columns in the blocks in row $\tau$ .
	$V_\tau$	$m \times k$	Basis for the rows in the blocks in column $\tau$ .
For each parent node $\tau$ :	$B_\tau$	$2k \times 2k$	Interactions between the children of $\tau$ .
	$U_\tau$	$2k \times k$	Basis for the columns in the (reduced) blocks in row $\tau$ .
	$V_\tau$	$2k \times k$	Basis for the rows in the (reduced) blocks in column $\tau$ .

FIGURE 5. An HBS matrix  $H$  associated with a tree  $\mathcal{T}$  is fully specified if the factors listed above are provided.

(1) *Assumption on ranks of off-diagonal blocks at the finest level:* For any two distinct leaf nodes  $\tau$  and  $\tau'$ , define the  $n \times n$  matrix

$$(11) \quad H_{\tau, \tau'} = H(I_\tau, I_{\tau'}).$$

Then there must exist matrices  $U_\tau$ ,  $V_{\tau'}$ , and  $\tilde{H}_{\tau, \tau'}$  such that

$$(12) \quad \begin{array}{cccc} H_{\tau, \tau'} & = & U_\tau & \tilde{H}_{\tau, \tau'} & V_{\tau'}^* \\ m \times m & & m \times k & k \times k & k \times m \end{array}$$

(2) *Assumption on ranks of off-diagonal blocks on level  $\ell = L - 1, L - 2, \dots, 1$ :* The rank assumption at level  $\ell$  is defined in terms of the blocks constructed on the next finer level  $\ell + 1$ : For any distinct nodes  $\tau$  and  $\tau'$  on level  $\ell$  with children  $\sigma_1, \sigma_2$  and  $\sigma'_1, \sigma'_2$ , respectively, define

$$(13) \quad H_{\tau, \tau'} = \begin{bmatrix} \tilde{H}_{\sigma_1, \sigma'_1} & \tilde{H}_{\sigma_1, \sigma'_2} \\ \tilde{H}_{\sigma_2, \sigma'_1} & \tilde{H}_{\sigma_2, \sigma'_2} \end{bmatrix}.$$

Then there must exist matrices  $U_\tau$ ,  $V_{\tau'}$ , and  $\tilde{H}_{\tau, \tau'}$  such that

$$(14) \quad \begin{array}{cccc} H_{\tau, \tau'} & = & U_\tau & \tilde{H}_{\tau, \tau'} & V_{\tau'}^* \\ 2k \times 2k & & 2k \times k & k \times k & k \times 2k \end{array}$$

An HBS matrix is now fully described if the basis matrices  $U_\tau$  and  $V_\tau$  are provided for each node  $\tau$ , and in addition, we are for each leaf  $\tau$  given the  $m \times m$  matrix

$$(15) \quad D_\tau = H(I_\tau, I_\tau),$$

and for each parent node  $\tau$  with children  $\sigma_1$  and  $\sigma_2$  we are given the  $2k \times 2k$  matrix

$$(16) \quad B_\tau = \begin{bmatrix} 0 & \tilde{H}_{\sigma_1, \sigma_2} \\ \tilde{H}_{\sigma_2, \sigma_1} & 0 \end{bmatrix}.$$

Observe in particular that the matrices  $\tilde{H}_{\sigma_1, \sigma_2}$  are only required when  $\{\sigma_1, \sigma_2\}$  forms a sibling pair. Figure 5 summarizes the required matrices.

**4.4. Telescoping factorization.** Given the matrices defined in the previous section, we define the following block diagonal factors:

$$(17) \quad \underline{\mathbf{D}}^{(\ell)} = \text{diag}(\mathbf{D}_\tau : \tau \text{ is a box on level } \ell), \quad \ell = 0, 1, \dots, L,$$

$$(18) \quad \underline{\mathbf{U}}^{(\ell)} = \text{diag}(\mathbf{U}_\tau : \tau \text{ is a box on level } \ell), \quad \ell = 1, 2, \dots, L,$$

$$(19) \quad \underline{\mathbf{V}}^{(\ell)} = \text{diag}(\mathbf{V}_\tau : \tau \text{ is a box on level } \ell), \quad \ell = 1, 2, \dots, L,$$

$$(20) \quad \underline{\mathbf{B}}^{(\ell)} = \text{diag}(\mathbf{B}_\tau : \tau \text{ is a box on level } \ell), \quad \ell = 0, 1, \dots, L-1, .$$

Furthermore, we let  $\tilde{\mathbf{H}}^{(\ell)}$  denote the block matrix whose diagonal blocks are zero, and whose off-diagonal blocks are the blocks  $\tilde{\mathbf{H}}_{\tau, \tau'}$  for all distinct  $\tau, \tau'$  on level  $\ell$ . With these definitions,

$$(21) \quad \begin{array}{c} \mathbf{H} \\ m 2^L \times n 2^L \end{array} = \begin{array}{c} \underline{\mathbf{U}}^{(L)} \\ m 2^L \times k 2^L \end{array} \begin{array}{c} \tilde{\mathbf{H}}^{(L)} \\ k 2^L \times k 2^L \end{array} \begin{array}{c} (\underline{\mathbf{V}}^{(L)})^* \\ k 2^L \times m 2^L \end{array} + \begin{array}{c} \underline{\mathbf{D}}^{(L)} \\ m 2^L \times m 2^L \end{array};$$

for  $\ell = L-1, L-2, \dots, 1$  we have

$$(22) \quad \begin{array}{c} \tilde{\mathbf{H}}^{(\ell+1)} \\ k 2^{\ell+1} \times k 2^{\ell+1} \end{array} = \begin{array}{c} \underline{\mathbf{U}}^{(\ell)} \\ k 2^{\ell+1} \times k 2^\ell \end{array} \begin{array}{c} \tilde{\mathbf{H}}^{(\ell)} \\ k 2^\ell \times k 2^\ell \end{array} \begin{array}{c} (\underline{\mathbf{V}}^{(\ell)})^* \\ k 2^\ell \times k 2^{\ell+1} \end{array} + \begin{array}{c} \underline{\mathbf{B}}^{(\ell)} \\ k 2^{\ell+1} \times k 2^{\ell+1} \end{array};$$

and finally

$$(23) \quad \tilde{\mathbf{H}}^{(1)} = \underline{\mathbf{B}}^{(0)}.$$

## 5. FAST ARITHMETIC OPERATIONS ON HBS MATRICES

Arithmetic operations involving dense HBS matrices of size  $N \times N$  can often be executed in  $O(N)$  operations. This fast matrix algebra is vital for achieving linear complexity in our direct solver. This section provides a brief introduction to the HBS matrix algebra. We describe the operations we need (inversion, addition, and low-rank update) in some detail for the single level ‘‘block separable’’ format. The generalization to the multi-level ‘‘hierarchically block separable’’ format is briefly described for the case of matrix inversion. A full description of all algorithms required is given in [7], which is related to the earlier work [4].

Before we start, we recall that a block separable matrix  $\mathbf{H}$  consisting of  $p \times p$  blocks, each of size  $m \times m$ , and with ‘‘HBS-rank’’  $k < m$ , admits the factorization

$$(24) \quad \begin{array}{c} \mathbf{H} \\ mp \times mp \end{array} = \begin{array}{c} \mathbf{U} \\ mp \times kp \end{array} \begin{array}{c} \tilde{\mathbf{H}} \\ kp \times kp \end{array} \begin{array}{c} \mathbf{V}^* \\ kp \times mp \end{array} + \begin{array}{c} \mathbf{D} \\ mp \times mp \end{array}.$$

**5.1. Inversion of a block separable matrix.** The decomposition (24) represents  $\mathbf{H}$  as a sum of one term  $\tilde{\mathbf{U}}\tilde{\mathbf{H}}\tilde{\mathbf{V}}^*$  that is ‘‘low rank,’’ and one term  $\mathbf{D}$  that is easily invertible (since it is block diagonal). By modifying the classical Woodbury formula for inversion of a matrix perturbed by the addition of a low-rank term, it can be shown that (see Lemma 3.1 of [8])

$$(25) \quad \mathbf{H}^{-1} = \mathbf{E}(\tilde{\mathbf{H}} + \hat{\mathbf{D}})^{-1}\mathbf{F}^* + \mathbf{G},$$

where

$$(26) \quad \hat{D} = (\mathbf{V}^* \mathbf{D}^{-1} \mathbf{U})^{-1},$$

$$(27) \quad \mathbf{E} = \mathbf{D}^{-1} \mathbf{U} \hat{D},$$

$$(28) \quad \mathbf{F} = (\hat{D} \mathbf{V}^* \mathbf{D}^{-1})^*,$$

$$(29) \quad \mathbf{G} = \mathbf{D}^{-1} - \mathbf{D}^{-1} \mathbf{U} \hat{D} \mathbf{V}^* \mathbf{D}^{-1},$$

assuming the inverses in formulas (25) — (29) all exist. Now observe that the matrices  $\hat{D}$ ,  $\mathbf{E}$ ,  $\mathbf{F}$ , and  $\mathbf{G}$  can all easily be computed since the formulas defining them involve only block-diagonal matrices. In consequence, (25) reduces the task of inverting the big (size  $mp \times mp$ ) matrix  $\mathbf{H}$  to the task of inverting the small (size  $kp \times kp$ ) matrix  $\tilde{\mathbf{H}} + \hat{D}$ .

When  $\mathbf{H}$  is not only “block separable”, but “hierarchically block separable”, the process can be repeated recursively by exploiting that  $\tilde{\mathbf{H}} + \hat{D}$  is itself amenable to accelerated inversion, etc. The resulting process is somewhat tricky to analyze, but leads to very clean codes. To illustrate, we include Algorithm 1 which shows the multi-level  $O(N)$  inversion algorithm for an HBS matrix  $\mathbf{H}$ . The algorithm takes as input the factors  $\{\mathbf{U}_\tau, \mathbf{V}_\tau, \mathbf{D}_\tau, \mathbf{B}_\tau\}_\tau$  representing  $\mathbf{H}$  (cf. Figure 5), and outputs an analogous set of factors  $\{\mathbf{E}_\tau, \mathbf{F}_\tau, \mathbf{G}_\tau\}_\tau$  representing  $\mathbf{H}^{-1}$ . With these factors, the matrix-vector multiplication  $\mathbf{y} = \mathbf{H}^{-1}\mathbf{x}$  can be executed via the procedure described in Algorithm 2.

**5.2. Addition of two block separable matrices.** Let  $\mathbf{H}^A$  and  $\mathbf{H}^B$  be block separable matrices with factorizations

$$\mathbf{H}^A = \mathbf{U}^A \tilde{\mathbf{H}}^A \mathbf{V}^{A*} + \mathbf{D}^A, \quad \text{and} \quad \mathbf{H}^B = \mathbf{U}^B \tilde{\mathbf{H}}^B \mathbf{V}^{B*} + \mathbf{D}^B.$$

Then  $\mathbf{H} = \mathbf{H}^A + \mathbf{H}^B$  can be written in block separable form via

$$(30) \quad \mathbf{H} = \mathbf{H}^A + \mathbf{H}^B = [\mathbf{U}^A \ \mathbf{U}^B] \begin{bmatrix} \tilde{\mathbf{H}}^A & 0 \\ 0 & \tilde{\mathbf{H}}^B \end{bmatrix} [\mathbf{V}^A \ \mathbf{V}^B]^* + (\mathbf{D}^A + \mathbf{D}^B).$$

To restore (30) to block separable form, permute the rows and columns of  $[\mathbf{U}^A \ \mathbf{U}^B]$  and  $[\mathbf{V}^A \ \mathbf{V}^B]$  to attain block diagonal form, then re-orthogonalize the diagonal blocks. This process in principle results in a matrix  $\mathbf{H}$  whose HBS-rank is the sum of the HBS-ranks of  $\mathbf{H}^A$  and  $\mathbf{H}^B$ . In practice, this rank increase can be combatted by numerically recompressing the basis matrices, and updating the middle factor as needed. For details, as well as the extension to a multi-level scheme, see [4, 7].

**5.3. Addition of a block separable matrix with a low rank matrix.** Let  $\mathbf{H}^B = \mathbf{Q}\mathbf{R}$  be a  $k$ -rank matrix where  $\mathbf{Q}$  and  $\mathbf{R}^*$  are of size  $mp \times k$ . We would like to add  $\mathbf{H}^B$  to the block separable matrix  $\mathbf{H}^A$ . Since we already know how to add two block separable matrices, we choose to rewrite  $\mathbf{H}^B$  in block separable form. Without loss of generality, assume  $\mathbf{Q}$  is orthogonal. Partition  $\mathbf{Q}$  into  $p$  blocks of size  $m \times k$ . The blocks make up the matrix  $\mathbf{U}^B$ . Likewise partition  $\mathbf{R}$  into  $p$  blocks of size  $k \times m$ . The block matrix  $\mathbf{D}^B$  has entries

ALGORITHM 1 (inversion of an HBS matrix)

Given factors  $\{U_\tau, V_\tau, D_\tau, B_\tau\}_\tau$  representing an HBS matrix  $H$ , this algorithm constructs factors  $\{E_\tau, F_\tau, G_\tau\}_\tau$  representing  $H^{-1}$ .

**loop** over all levels, finer to coarser,  $\ell = L, L - 1, \dots, 1$

**loop** over all boxes  $\tau$  on level  $\ell$ ,

**if**  $\tau$  is a leaf node

$\tilde{D}_\tau = D_\tau$

**else**

Let  $\sigma_1$  and  $\sigma_2$  denote the children of  $\tau$ .

$\tilde{D}_\tau = \begin{bmatrix} \hat{D}_{\sigma_1} & B_{\sigma_1, \sigma_2} \\ B_{\sigma_2, \sigma_1} & \hat{D}_{\sigma_2} \end{bmatrix}$

**end if**

$\hat{D}_\tau = (V_\tau^* \tilde{D}_\tau^{-1} U_\tau)^{-1}$ .

$E_\tau = \tilde{D}_\tau^{-1} U_\tau \hat{D}_\tau$ .

$F_\tau^* = \hat{D}_\tau V_\tau^* \tilde{D}_\tau^{-1}$ .

$G_\tau = \tilde{D}_\tau^{-1} - \tilde{D}_\tau^{-1} U_\tau \hat{D}_\tau V_\tau^* \tilde{D}_\tau^{-1}$ .

**end loop**

**end loop**

$G_1 = \begin{bmatrix} \hat{D}_2 & B_{2,3} \\ B_{3,2} & \hat{D}_3 \end{bmatrix}^{-1}$ .

$D_\tau = Q_\tau R_\tau$  for  $\tau = 1, \dots, p$ . To construct the matrices  $V^B$ , for each  $\tau = 1, \dots, p$ , the matrix  $R_\tau$  is factorized into  $\tilde{R}_\tau V_\tau^*$  where the matrix  $V_\tau$  is orthogonal. The matrices  $\tilde{R}_\tau$  make up the entries of  $\tilde{H}^B$ .

## 6. ACCELERATING THE NESTED DISSECTION ALGORITHM

In this section, we apply the structured matrix techniques introduced in Sections 4 and 5 to reduce the complexity of the solver of Section 3 from  $O(N^{1.5})$  to  $O(N)$ . The key task that we need to accelerate is the construction of the Schur complement for a parent box from the Schur complements of its two children. The formula that needs to be evaluated is, cf. (8),

$$(31) \quad S = \begin{bmatrix} S_{11} & A_{12} \\ A_{21} & S_{22} \end{bmatrix} - \begin{bmatrix} S_{13} & A_{14} \\ A_{23} & S_{24} \end{bmatrix} \begin{bmatrix} S_{33} & A_{34} \\ A_{43} & S_{44} \end{bmatrix}^{-1} \begin{bmatrix} S_{31} & A_{32} \\ A_{41} & S_{42} \end{bmatrix}.$$

The acceleration can be broken into three steps which utilize important properties of each submatrix.

**Step 1** The inverse in equation (31) never needs to be constructed. Instead the solution of

$$(32) \quad \begin{bmatrix} S_{33} & A_{34} \\ A_{43} & S_{44} \end{bmatrix} \begin{bmatrix} X_3 \\ X_4 \end{bmatrix} = \begin{bmatrix} Z_3 \\ Z_4 \end{bmatrix},$$

## ALGORITHM 2 (application of inverse)

Given  $\mathbf{x}$ , compute  $\mathbf{y} = \mathbf{H}^{-1} \mathbf{x}$  using the compressed representation of  $\mathbf{H}^{-1}$  resulting from Algorithm 1.

**loop** over all leaf boxes  $\tau$

$$\hat{\mathbf{x}}_\tau = \mathbf{F}_\tau^* \mathbf{x}(I_\tau).$$

**end loop**

**loop** over all levels, finer to coarser,  $\ell = L, L-1, \dots, 1$

**loop** over all parent boxes  $\tau$  on level  $\ell$ ,

Let  $\sigma_1$  and  $\sigma_2$  denote the children of  $\tau$ .

$$\hat{\mathbf{x}}_\tau = \mathbf{F}_\tau^* \begin{bmatrix} \hat{\mathbf{x}}_{\sigma_1} \\ \hat{\mathbf{x}}_{\sigma_2} \end{bmatrix}.$$

**end loop**

**end loop**

$$\begin{bmatrix} \hat{\mathbf{y}}_2 \\ \hat{\mathbf{y}}_3 \end{bmatrix} = \mathbf{G}_1 \begin{bmatrix} \hat{\mathbf{x}}_2 \\ \hat{\mathbf{x}}_3 \end{bmatrix}.$$

**loop** over all levels, coarser to finer,  $\ell = 1, 2, \dots, L-1$

**loop** over all parent boxes  $\tau$  on level  $\ell$

Let  $\sigma_1$  and  $\sigma_2$  denote the children of  $\tau$ .

$$\begin{bmatrix} \hat{\mathbf{y}}_{\sigma_1} \\ \hat{\mathbf{y}}_{\sigma_2} \end{bmatrix} = \mathbf{E}_\tau \hat{\mathbf{x}}_\tau + \mathbf{G}_\tau \begin{bmatrix} \hat{\mathbf{x}}_{\sigma_1} \\ \hat{\mathbf{x}}_{\sigma_2} \end{bmatrix}.$$

**end loop**

**end loop**

**loop** over all leaf boxes  $\tau$

$$\mathbf{y}(I_\tau) = \mathbf{E}_\tau \hat{\mathbf{q}}_\tau + \mathbf{G}_\tau \mathbf{x}(I_\tau).$$

**end loop**

can be found by rapidly via a block solve. Then  $\begin{bmatrix} \mathbf{X}_3 \\ \mathbf{X}_4 \end{bmatrix}$  is given by

$$\mathbf{X}_4 = (\mathbf{S}_{44} - \mathbf{A}_{43} \mathbf{S}_{33}^{-1} \mathbf{A}_{34})^{-1} (\mathbf{Z}_4 - \mathbf{A}_{43} \mathbf{S}_{33}^{-1} \mathbf{Z}_3)$$

and

$$\mathbf{X}_3 = \mathbf{S}_{33}^{-1} \mathbf{Z}_3 - \mathbf{S}_{33}^{-1} \mathbf{A}_{34} \mathbf{X}_4.$$

Since  $\mathbf{S}_{33}$  is HBS, an approximation of its inverse can be constructed and applied rapidly. The matrix  $\mathbf{A}_{43} \mathbf{S}_{33}^{-1} \mathbf{A}_{34}$  is also HBS, since  $\mathbf{A}_{43}$  and  $\mathbf{A}_{34}$  are anti-diagonal matrices (ie. all the entries are zero except those on the diagonal going from the lower left corner to the upper right corner). Hence  $\mathbf{S}_{44} - \mathbf{A}_{43} \mathbf{S}_{33}^{-1} \mathbf{A}_{34}$  can be added quickly. The resulting matrix is HBS and can be inverted with linear scaling computational cost.

Let  $\begin{bmatrix} X_{31} & X_{32} \\ X_{41} & X_{42} \end{bmatrix}$  denote the result of applying the block inverse to  $\begin{bmatrix} S_{31} & A_{32} \\ A_{41} & S_{42} \end{bmatrix}$ .

**Step 2** The matrices  $S_{13}$ , and  $S_{24}$  are low rank, thus we can rewrite the matrices in their low rank factored form as  $L_{13}R_{13}$  and  $L_{24}R_{24}$ . Using this notation, the second term in (31) can be expressed in a low rank factored form

$$(33) \quad \begin{bmatrix} S_{13} & A_{14} \\ A_{23} & S_{24} \end{bmatrix} \begin{bmatrix} X_{31} & X_{32} \\ X_{41} & X_{42} \end{bmatrix} = \begin{bmatrix} L_{13}R_{13}X_{31} + A_{14}X_{41} & L_{13}R_{13}X_{32} + A_{14}X_{42} \\ A_{23}X_{31} + L_{24}R_{24}X_{41} & A_{23}X_{32} + L_{24}R_{24}X_{42} \end{bmatrix}.$$

Since all the matrices  $A_{jk}$  are very sparse, the four blocks on the right hand side of (33) are of low rank. (Recall in the case of the five point stencil, the matrices  $A_{14}$  and  $A_{23}$  are zero).

Let  $\begin{bmatrix} L_{11}R_{11} & L_{12}R_{12} \\ L_{21}R_{21} & L_{22}R_{22} \end{bmatrix}$  denote the low rank factorization of the blocks in (33).

**Step 3** Now we add the two terms that comprise the Schur complement

$$\begin{bmatrix} S_{11} & A_{12} \\ A_{21} & S_{22} \end{bmatrix} - \begin{bmatrix} L_{11}R_{11} & L_{12}R_{12} \\ L_{21}R_{21} & L_{22}R_{22} \end{bmatrix}.$$

The diagonal block entries are HBS + low rank which is computed via Algorithms 3 and 2. The off-diagonal blocks are low rank with a very sparse update which is also low rank. The result is one HBS matrix.

**Remark 6.1.** As a practical matter, structured matrix algebra should not be introduced until the Schur complements get fairly large (roughly of size  $1000 \times 1000$  or so). This means that at the lower levels, formula (31) is evaluated using dense matrix algebra for all matrices  $S_{i,j}$ .

## 7. NUMERICAL EXPERIMENTS

In this section, we illustrate the capabilities of the proposed method for constructing solution operators for problems of the form

$$(34) \quad \begin{cases} -\Delta u(\mathbf{x}) + b(\mathbf{x})u_x(\mathbf{x}) + c(\mathbf{x})u_y(\mathbf{x}) + d(\mathbf{x})u(\mathbf{x}) = f(\mathbf{x}), & \mathbf{x} \in \Omega = [0, 1]^2, \\ u(\mathbf{x}) = g(\mathbf{x}), & \mathbf{x} \in \Gamma, \end{cases}$$

where  $b$ ,  $c$ ,  $d$ , and  $f$  are functions defined on  $\Omega$ , and the boundary data  $g$  is defined on  $\Gamma$ . Section 7.1 investigates the asymptotic complexity of the direct solver for several different differential operators (Laplace, Helmholtz, convection-diffusion, etc.) for the case where the body load is zero ( $f = 0$ ). It also reports on the accuracy for each case. Section 7.2 reports the execution times of the build and the solve stages of the direct solver. Section 7.3 reports on the performance of the method for a problem with localized body loads.

For all problems, the domain is discretized with a uniform grid of  $n \times n$  points so that the grid spacing is  $h = 1/(n - 1)$ . We let  $N = n^2$  denote the total number of nodes. Equation (34) is discretized with the finite



difference scheme corresponding to the five point stencil. For example, when a node  $k$  is in the interior of  $\Omega$ , the discretization of the differential operator in (34) is

$$\frac{1}{h^2} [4u(k) - u(k_n) - u(k_s) - u(k_w) - u(k_e)] + \frac{1}{h} b(k) [u(k_e) - u(k_w)] + \frac{1}{h} c(k) [u(k_n) - u(k_s)] + d(k)u(k),$$

where  $k_e, k_n, k_w, k_s$  denote the grid points to the “east”, “north”, “west”, and “south” of  $k$ , respectively. The HBS matrix algebra was run with a local tolerance of  $\varepsilon = 10^{-7}$ .

All experiments are executed on a Lenovo laptop computer with a 2.4GHz Intel i5 processor and 8GB of RAM. The method was implemented in Matlab, which we judged adequate since the main purpose of the experiments is to substantiate our claims in regards to asymptotic complexity. It should be noted, however, that even this non-optimized code runs quite fast, see, e.g., Table 4.

Recall that the approximate solution (or Dirichlet-to-Neumann) operator  $\mathbf{G}$  is the inverse of the Schur complement  $\mathbf{S}$  for the full domain, see Section 3.1.

**7.1. Range of problems with optimal scaling.** The proposed method for constructing Dirichlet-to-Neumann operators has been applied to several problems to investigate its asymptotic complexity. The problems are:

- *Laplace*: Let  $b(\mathbf{x}) = c(\mathbf{x}) = d(\mathbf{x}) = 0$ .
- *Diffusion-Convection I*: Let  $c(\mathbf{x}) = d(\mathbf{x}) = 0$  and the convection in the  $x$  direction be constant:  $b(\mathbf{x}) = 100$ .
- *Diffusion-Convection II*: Same as *Diffusion-Convection I*, but with  $b(\mathbf{x}) = 1000$ .
- *Diffusion-convection III*: Introduce a divergence free convection field by setting  $b(\mathbf{x}) = 125 \cos(4\pi y)$  and  $c(\mathbf{x}) = 125 \sin(4\pi x)$ , and  $d(\mathbf{x}) = 0$ .
- *Diffusion-convection IV*: Introduce a convection field with sources and sinks by setting Let  $b(\mathbf{x}) = 125 \cos(4\pi x)$ ,  $c(\mathbf{x}) = 125 \sin(4\pi y)$ , and  $d(\mathbf{x}) = 0$ .
- *Helmholtz I*: Consider the Helmholtz equation corresponding to a domain that is roughly  $1.5 \times 1.5$  wavelengths large:  $b(\mathbf{x}) = c(\mathbf{x}) = 0$  and  $d(\mathbf{x}) = -100$ .
- *Helmholtz II*: Consider the Helmholtz equation corresponding to a domain that is roughly  $10 \times 10$  wavelengths large:  $b(\mathbf{x}) = c(\mathbf{x}) = 0$  and  $d(\mathbf{x}) = -4005$ .
- *Helmholtz III*: Consider the Helmholtz equation near a resonance:  $b(\mathbf{x}) = c(\mathbf{x}) = 0$  and  $d(\mathbf{x}) = -\lambda_{10} + 10^{-5}$ , where  $\lambda_{10}$  is the tenth eigenvalue of the discrete Laplace operator (note that these are known analytically).
- *Helmholtz IV*: Consider a sequence of Helmholtz problems where the wave-number is increased to keep a constant 40 points per wave-length:  $b(\mathbf{x}) = c(\mathbf{x}) = 0$  and  $d(\mathbf{x}) = -\left(\frac{2\pi n}{40}\right)^2$ .
- *Random Laplacian I*: Let the matrix  $\mathbf{A}$  reflect an elliptic equilibrium problem on a network instead of a continuum PDE. In this case, the network is the square grid where each link is assigned a random

*conductivity* between varying between 1 and 2. The potential at any single node is the weighted average of the potentials of its four neighbors, where the weights are the conductivities.

- *Random Laplacian II*: Same as *Random Laplacian I*, but now the conductivities vary between 1 and 1000.

Table 2 reports the amount of memory  $M(n)$  in MB required to store the Dirichlet-to-Neumann operator  $\mathbf{G}$  for each problem; it also reports the fraction  $M(n)/n$ . Our claim in regards to compressibility amounts to a prediction that  $M(n)/n$  will remain stable as  $n$  grows for all problems, except for Helmholtz IV. Table 2 demonstrates that this scaling holds true in the range  $n = [256, 512, 1024, 2048]$ .

Table 3 reports two errors measured on a grid of size  $1024 \times 1024$ :

$e_1$  - the relative  $l^2$ -error in the vector  $\mathbf{G}\mathbf{r}$  where  $\mathbf{r}$  is a unit vector of random direction

$e_2$  - the relative  $l^2$ -error in the vector  $\mathbf{G}\mathbf{r}$  where  $\mathbf{r}$  is smooth.

The exact value of  $\mathbf{G}\mathbf{r}$  was found by using GMRES to solve the full original linear system  $\mathbf{A}\mathbf{x} = \hat{\mathbf{r}}$ , where  $\hat{\mathbf{r}}$  is a vector of length  $n^2$  such that  $\hat{\mathbf{r}}|_{\Gamma} = \mathbf{r}$  and  $\hat{\mathbf{r}}|_{\Omega \setminus \Gamma} = 0$ . A slight loss in accuracy is observed for Helmholtz I, IV and Random II problems. There is a substantial loss in accuracy for the Helmholtz III problem. This is to be expected since the matrix  $\mathbf{A}$  is close to being numerically singular.

<i>Problem</i>	$n = 256$	$n = 512$	$n = 1024$	$n = 2048$
<i>Laplace</i>	0.83 (3.2e-3)	1.62 (3.2e-3)	3.18 (3.1e-3)	6.27 (3.1e-3)
<i>DiffConv I</i>	0.91 (3.5e-3)	1.75 (3.4e-3)	3.32 (3.2e-3)	6.52 (3.2e-3)
<i>DiffConv II</i>	1.10 (4.3e-3)	1.84 (3.6e-3)	3.62 (3.5e-3)	6.87 (3.4e-3)
<i>DiffConv III</i>	0.86 (3.4e-3)	1.70 (3.3e-3)	3.32 (3.2e-3)	6.55 (3.3e-3)
<i>DiffConv IV</i>	0.97 (3.8e-3)	1.83 (3.6e-3)	3.43 (3.3e-3)	6.59 (3.2e-3)
<i>Helmholtz I</i>	0.86 (3.4e-3)	1.67 (3.3e-3)	3.25 (3.2e-3)	6.34 (3.1e-3)
<i>Helmholtz II</i>	1.04 (4.1e-3)	1.91 (3.7e-3)	3.56 (3.5e-3)	6.78 (3.3e-3)
<i>Helmholtz III</i>	0.86 (3.4e-3)	1.67 (3.3e-3)	3.29 (3.2e-3)	6.42 (3.1e-3)
<i>Helmholtz IV</i>	0.89 (3.5e-3)	1.74 (3.4e-3)	3.59 (3.5e-3)	7.89 (3.9e-3)
<i>Random I</i>	0.83 (3.2e-3)	1.64 (3.2e-3)	3.22 (3.1e-3)	6.34 (3.1e-3)
<i>Random II</i>	0.82 (3.2e-3)	1.64 (3.2e-3)	3.23 (3.2e-3)	6.36 (3.1e-3)

TABLE 2. Memory  $M(n)$  in MB required to store the solution operator for the problems listed in Section 7.1. The quantity  $\frac{M(n)}{n}$  is reported in parenthesis.

**7.2. Performance.** In this section we report the computational times required for the experiments that were described in Section 7.1, for grids of size  $512 \times 512$  to  $4096 \times 4096$ . Since the times were very similar across most experiments, we report only those for *Laplace*, which represents the “typical” times observed, and for *Helmholtz IV*, which was the most challenging and slowest of all the experiments conducted. Table 4 reports:

<i>Problem</i>	$e_1$	$e_2$
<i>Laplace</i>	6.3e-7	3.6e-7
<i>DiffConv I</i>	1.5e-6	1.3e-6
<i>DiffConv II</i>	8.7e-6	8.2e-6
<i>DiffConv III</i>	5.6e-7	3.4e-7
<i>DiffConv IV</i>	4.1e-8	4.1e-8
<i>Helmholtz I</i>	1.4e-4	4.8e-7
<i>Helmholtz II</i>	1.1e-6	5.1e-6
<i>Helmholtz III</i>	1.2e-5	5.7e-4
<i>Helmholtz IV</i>	8.2e-4	1.2e-3
<i>Random I</i>	1.8e-7	1.2e-7
<i>Random II</i>	1.4e-5	8.1e-6

TABLE 3. Errors  $e_1$  and  $e_2$  for the solution operator for the problems listed in Section 7.1.

$T_{\text{build}}$  - the time in seconds for constructing the Dirichlet-to-Neumann operator,

$T_{\text{solve}}$  - the time in seconds for applying the Dirichlet-to-Neumann operator to a vector.

Let us draw the reader’s attention to some interesting results in Table 4:

- A principal claim we make in terms of performance of the proposed method is that after an initial pre-computation in which the solution operator is built, the time  $T_{\text{solve}}$  required to process a new vector of Dirichlet data is small. Table 4 clearly bears out our claim that  $T_{\text{solve}}$  scales linearly with *the number of points on the boundary*, in other words  $T_{\text{solve}} \sim N^{0.5}$ . Moreover, the scaling constant turns out to be small, for a grid of size  $4096 \times 4096$ , the solve time is only 0.1 seconds.
- The other key claim made is that the time to build the solution operator in the first place scales linearly with the number of points in the grid, in other words  $T_{\text{build}} \sim N$ . Table 4 shows that for grids holding between 250k and 16M nodes, the build time in fact scales sub-linearly. Eventually, linear complexity must of course kick in, but it is interesting that it has not yet done so even for a grid holding over 16M nodes.
- For the example *Helmholtz IV* we did not predict linear complexity. This problem models wave-propagation in such a way that as  $n$  grows, the number of wave-lengths along a side of the domain grows proportionally. This will eventually destroy the rank-structure in the Schur complements that we rely on to reduce the  $O(N^{1.5})$  scaling of classical nested dissection down to  $O(N)$ . Now what is interesting is that while the *predicted* complexity is  $T_{\text{build}} \sim N^{1.5}$ , the *observed* complexity is only  $T_{\text{build}} \sim N$ . We expect that the predicted asymptotic scaling will eventually assert itself, but it is to us remarkable that it has not yet done so given that the largest domain with 16M nodes represents a physical problem of size  $100 \times 100$  wavelengths.

$N$	<i>Laplace</i>		<i>Helmholtz IV</i>	
	$T_{\text{build}}$ (sec)	$T_{\text{solve}}$ (sec)	$T_{\text{build}}$ (sec)	$T_{\text{solve}}$ (sec)
$512^2$	13.44	0.013	50.78	0.013
$1024^2$	45.25	0.027	193.58	0.027
$2048^2$	135.01	0.058	765.35	0.056
$4096^2$	450.73	0.107	3167.56	0.115

TABLE 4. Times for the approximation of the Dirichlet-to-Neumann operator for the *Laplace* and *Helmholtz IV* problems via the accelerated nested dissection method.

**7.3. Performance with body loads.** In this experiment, the *Random Laplacian I* problem is solved in a situation with a non-zero body load  $f$ . We assume however that the body load is restricted to a small number  $N_{\text{body}}$  of nodes in the interior. The locations of these nodes is assumed to be fixed. Our objective is now to construct a solution operator that constructs the vector of fluxes  $\mathbf{v}$  on the boundary (the discrete “Neumann data”) given a vector  $\mathbf{g}$  of Dirichlet data, and a vector  $\hat{\mathbf{f}} \in \mathbb{R}^{N_{\text{body}}}$  of body loads at the pre-scribed nodes. This solution operator has two terms as follows:

$$(35) \quad \begin{array}{ccccccc} \mathbf{v} & = & \mathbf{G} & \mathbf{g} & + & \mathbf{F} & \hat{\mathbf{f}}, \\ N_{\text{boundary}} \times 1 & & N_{\text{boundary}} \times N_{\text{boundary}} & N_{\text{boundary}} \times 1 & & N_{\text{boundary}} \times N_{\text{body}} & N_{\text{body}} \times 1 \end{array}$$

where  $N_{\text{boundary}} = 4(n - 1)$  denotes the number of points on the boundary. The matrix  $\mathbf{G}$  is our by now familiar discrete Dirichlet-to-Neumann operator; it is constructed in HBS form. The matrix  $\mathbf{F}$  is a new solution operator that maps the interior body load to boundary fluxes. Since  $N_{\text{body}}$  is small, the matrix  $\mathbf{F}$  is built in uncompressed form, and then approximated by a low-rank factorization.

Table 5 reports the computational times required to build the solution operators  $\mathbf{F}$  and  $\mathbf{G}$  in (35) for several different grid sizes and different values of  $N_{\text{body}}$ . The table also reports the relative errors when  $N_{\text{body}}$  random body loads are placed in a localized area inside the domain. Notice that for a small number of body loads the cost is close to that of solving a pure boundary value problem. As expected the computational cost grows as the number of body loads is increased.

**Remark 7.1.** In this section, we considered a special case where the body load  $\mathbf{f}$  is restricted to a small number of internal nodes. For the general case where the body load  $\mathbf{f}$  is supported on the entire domain, solution operators like (35) can still be constructed. In this case, the matrix  $\mathbf{F}$  is of size  $N_{\text{boundary}} \times N$ , and should be constructed in a data-sparse format analogous to the HBS format. This operator can be both built and applied in  $O(N)$  operations.

$N$	$N_{\text{body}}$	$T_{\text{build}}$	$T_{\text{solve}}$	$\epsilon_{\text{rel}}$
512 <sup>2</sup>	10	13.09	0.013	1.02e-6
	100	13.25	0.013	4.55e-7
	1000	43.21	0.015	3.42e-7
1024 <sup>2</sup>	10	47.33	0.027	1.23e-6
	100	48.89	0.027	6.46e-7
	1000	163.05	0.029	4.35e-7
2048 <sup>2</sup>	10	256.57	0.55	-
	100	268.27	0.58	-
	1000	713.55	0.059	-

TABLE 5. Times for building the solution operators and applying the Dirichlet-to-Neumann operator when  $N_{\text{body}}$  body loads are randomly distributed in the domain. The relative error  $\epsilon_{\text{rel}}$  in the solution is also reported.

## 8. CONCLUSIONS AND GENERALIZATIONS

This paper presents a fast method for constructing the Dirichlet-to-Neumann operator for elliptic problems with no body loads. Numerical results indicate that the method scales linearly with the number of discretization points  $N$  for a variety of problems. Since application of the solution operator scales linearly with the number of boundary points (typically  $O(N^{1/2})$ ), constructing the solution for multiple right-hand sides is essentially free once the Dirichlet-to-Neumann operator is built. For a problem involving approximately 16 million unknowns, it takes about 8 minutes to build the solution operator, and 0.1 seconds to apply it to a right-hand side.

The fast direct solver described here relies on the intermediate dense matrices being compressible in the sense of being either of low rank, or having the HBS structure described in Section 4. It is currently not well understood exactly when this holds, but the numerical experiments in Section 7 indicate that the property is remarkably stable across a broad range of test problems.

In the interest of concision, this paper considered only an operator discretized by a five-point stencil on a regular square grid. However, the scheme does not inherently depend on the special form of either the stencil or the grid. We expect that the generalization to other domains and other discretizations in 2D should in principle be unproblematic, as long as the computational stencil is not too large. (Fast construction of LU-decompositions of the stiffness operator on somewhat general grids is reported in [12].)

The scheme can also be generalized to problems in three dimensions; the simplistic implementation described here would have  $O(N^{3/2})$  complexity for the build stage, and  $O(N^{2/3})$  complexity for the solve stage. Given that classical nested dissection in 3D has complexity  $O(N^2)$  and  $O(N^{4/3})$  for the build and solve stages, this is a substantial gain, especially for the solve stage. In principle, one could build a scheme that uses accelerated

matrix algebra internally inside the HBS representation to attain  $O(N)$  complexity, but this would require significant work beyond that described in this paper.

#### ACKNOWLEDGEMENTS:

The work reported was supported by NSF grants DMS0748488 and DMS0941476.

#### REFERENCES

1. S. Börm, *Approximation of solution operators of elliptic partial differential equations by  $\mathcal{H}$ - and  $\mathcal{H}^2$ -matrices*, Tech. Report 85/2007, Max Planck Institute, 2007.
2. S. Chandrasekaran and M. Gu, *A divide-and-conquer algorithm for the eigendecomposition of symmetric block-diagonal plus semiseparable matrices*, Numer. Math. **96** (2004), no. 4, 723–731.
3. S. Chandrasekaran, M. Gu, X.S. Li, and J. Xia, *Superfast multifrontal method for large structured linear systems of equations*, SIAM J. Matrix Anal. Appl. **31** (2009), 1382–1411.
4. S. Chandrasekaran, M. Gu, X.S. Li, and J. Xia, *Fast algorithms for hierarchically semiseparable matrices*, Numer. Linear Algebra Appl. **17** (2010), 953–976.
5. S. C. Eisenstat, M. H. Schultz, and A. H. Sherman, *Applications of an element model for Gaussian elimination*, Sparse Matrix Computations (New York) (J. R. Bunch and D. J. Rose, eds.), Academic Press, 1976, pp. 85–96.
6. A. George, *Nested dissection of a regular finite element mesh*, SIAM J. Numer. Anal. **10** (1973), 345–363.
7. A. Gillman, *Fast direct solvers for elliptic partial differential equations*, Ph.D. thesis, University of Colorado at Boulder, Applied Mathematics, 2011.
8. A. Gillman, P. Young, and P.G. Martinsson, *A direct solver with  $o(n)$  complexity for integral equations on one-dimensional domains*, Frontiers of Mathematics in China **7** (2012), no. 2, 217–247.
9. W. Hackbusch, *A sparse matrix arithmetic based on  $H$ -matrices; Part I: Introduction to  $H$ -matrices*, Computing **62** (1999), 89–108.
10. R. Kriemann L. Grasedyck and S. Le Borne, *Domain decomposition based  $\mathcal{H}$ -LU preconditioning*, Numer. Math. **112** (2009), no. 4, 565–600. MR MR2507619 (2010e:65200)
11. P.G. Martinsson, *A fast direct solver for a class of elliptic partial differential equations*, J. Sci. Comput. **38** (2009), no. 3, 316–330. MR MR2475654 (2010c:65041)
12. P. Schmitz and L. Ying, *A fast direct solver for elliptic problems on general meshes in 2d*, (2010), To appear in J. Comput. Phys.
13. Z. Sheng, P. Dewilde, and S. Chandrasekaran, *Algorithms to solve hierarchically semi-separable systems*, System theory, the Schur algorithm and multidimensional analysis, Oper. Theory Adv. Appl., vol. 176, Birkhäuser, Basel, 2007, pp. 255–294.

